Dalton Transactions

ROYAL SOCIETY OF CHEMISTRY

COMMUNICATION

View Article Online
View Journal | View Issue

Cite this: *Dalton Trans.*, 2026, **55**, 102

Received 6th December 2025,
Accepted 8th December 2025

DOI: 10.1039/d5dt02924d

rsc.li/dalton

Dehydrogenation of ammonia borane employing an air-stable, phosphine-free molecular nickel pincer catalyst

Bijan Mondal,† Aisa Mohanty† and Prosenjit Daw *

Herein, we report an air-stable, phosphine-free nickel catalyst supported by an NNN-based functionalized terpyridine ligand that enables the selective dehydrogenation of ammonia borane (AB). Operating under mild reaction conditions with low catalyst loading, achieves up to 2.58 equiv. of hydrogen evolution, while directing the reaction pathway toward borazine (BZ) formation.

1. Introduction

Developing safe, efficient, and high-capacity hydrogen storage materials remains a key challenge in the pursuit of clean energy technologies. Among the available candidates, ammonia borane (AB) is an attractive candidate owing to its high hydrogen content (19.6 wt%), air stability, low cost, and commercial availability, making it particularly promising for proton exchange membrane (PEM) fuel cells and hydrogen-powered transportation.[1,2] However, in the presence of the strong N–H···H–B dihydrogen bonding in AB, thermal decomposition occurs at around 90 °C, limiting its direct applicability.[3] To overcome this limitation, extensive efforts have focused on homogeneous transition metal catalysts that enable AB dehydrogenation under mild reaction conditions, with improved hydrogen release efficiency and selective formation of oligomeric species such as borazine (BZ), alongside two equiv. of hydrogen evolution. It can further convert into polyborazine (PBZ, a B–N coupled adduct), accompanied by the release of H_2 (Scheme 1a).[4] The released BZ serves as a versatile synthon for B–N-based oligomers and polymers with applications in ceramics, gas storage and separation, and supramolecular systems.[5]

In this regard, homogeneous transition metal complexes based on noble metals such as Ir, Ru, Pd, Rh, and Re have shown excellent performance, delivering high rates and selective formation of BZ or PBZ under optimised reaction conditions.[4,6–12] More recently, attention has shifted toward base-metal catalysts and organocatalysts[13,14] as cost-effective and sustainable alternatives. In line with this, iron-based complexes with diverse ligand architectures have been widely investigated, with a range of 1 to 2.5 equiv. of H_2 gas production, while cobalt-based catalysts have also demonstrated efficient AB dehydrogenation, producing 1 to 2 equiv. of H_2 gas alongside boron-containing oligomeric products such as B-(cyclodiborazanyl)-amine borane (BCDB)/B-(cyclotriborazanyl)amine-borane (BCTB), cyclotriborazine (CTB), BZ, and PBZ.[15–23] Notably, among the nickel-based systems, Baker and coworkers introduced the only report of the combination of $Ni(cod)_2$ precursors with an NHC carbene ligand, which achieved more

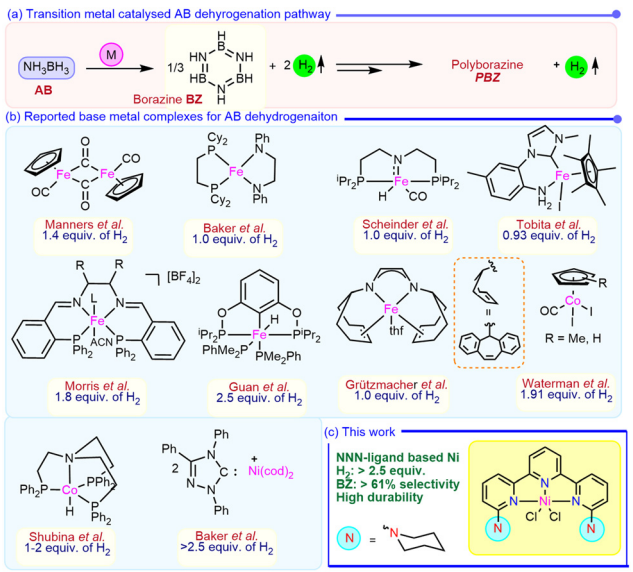

Scheme 1 (a) Transition metal catalysed AB dehydrogenation pathway; (b) reported base metal complexes for AB dehydrogenation; and (c) this work.

Department of Chemical Sciences, Indian Institute of Science Education and Research Berhampur, Transit Campus (Govt. ITI Building), Engg. School Junction, Berhampur 760010, Odisha, India. E-mail: pdaw@iiserbpr.ac.in

† These authors contributed equally.

than 2.5 equiv. of H_2 release with BZ and PBZ as end products from AB dehydrogenation (Scheme 1b).[24]

Despite the effectiveness of base-metal catalysts, their use is limited by BN polymer formation, unquantified BZ formation, the need for external base-additives, and instability from nanoparticle formation. To overcome these challenges, robust NNN ligands might offer a more sustainable alternative by replacing air- and moisture-sensitive ligands. In this work, we report an air-stable, homogeneous, designed molecular Ni-based complex supported by a functionalized terpyridine NNN ligand, which efficiently catalyses AB dehydrogenation. The catalytic protocol delivers up to 2.58 equiv. of H_2 and selectivity toward BZ, while maintaining durability up to eight catalytic cycles with a high catalytic TON (Scheme 1c).

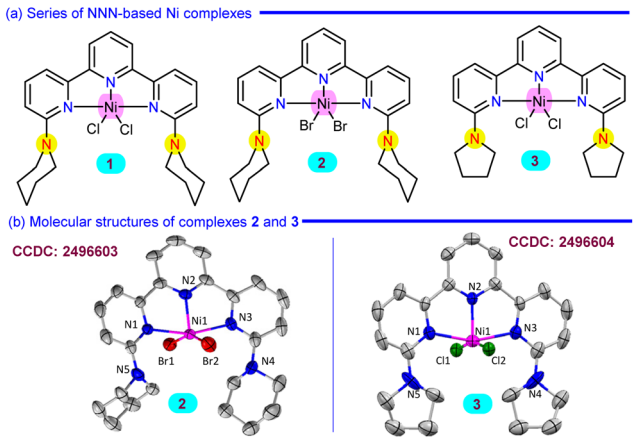

Scheme 2 (a) Series of NNN-based Ni complexes and (b) molecular structures of complexes **2** and **3**.

2. Results and discussion

Building on our previous work, Ni complexes **1**, the chloro analogue, and **2**, the bromo analogue, both featuring a piperidine-functionalized terpyridine ligand (**L1**),[25] were synthesised and fully characterised.[26] In a similar way, a pyrrolidine functionalized terpyridine ligand **L2** was synthesised, and the corresponding Ni complex **3** was prepared using $NiCl_2(PPh_3)_2$ in THF, and spectroscopically characterised (Scheme 2a). Both complexes **2** and **3** displayed a distorted square pyramidal geometry around the Ni centre with the rigid binding of the functionalized NNN ligand backbone, observed from single crystal X-ray analysis (Scheme 2b, see SI, sections 9.1 and 9.2).

Inspired by the excellent catalytic reactivity of Ni complexes **1** and **2** in the transfer hydrogenation of azoarenes using AB in ethanol as the hydrogenating source,[26] we intended to study the dehydrogenation of AB as a hydrogen-rich substrate directly to monitor the hydrogen evolution using these designed Ni complexes (Table 1). Initially using AB (1 mmol) in the presence of complex **1** (1 mol%) at 60 °C for 12 h as optimal conditions resulted in 42 mL (1.86 equiv.) of H_2 gas with 29% of BZ formation, detected from the ^{11}B spectroscopy at 31.03 ppm (d) using $NaBPh_4$ (0.01 mmol) as an internal standard (entry 1). Along with the BZ, other oligomeric species such as BCTB, μ-amidodiborane (μ-ADB) and PBZ were also observed in the ^{11}B spectra (see SI, Fig. S24).[16] The liberated H_2 gas was collected using an inverted water burette, and its purity was verified by gas chromatography and further confirmed through a chemical technique by performing Pd/C-catalyzed hydrogenation of styrene to ethylbenzene (see SI, section 7, Fig. S11).[27] However, instead of AB, utilising dimethyl ammonia borane ($NMe_2H{\cdot}BH_3$), only 6 mL of H_2 or

Table 1 Optimization of the catalytic dehydrogenation of AB using Ni complexes[a]

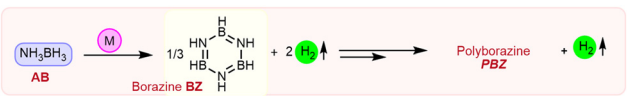

Entry	Ni catalyst	Solvent	Temp. (°C)	Time (h)	H_2 volume in mL (equiv.)	BZ (%)
1	**1**	THF	60	12	42 (1.86)	29
2	**2**	THF	60	12	42 (1.86)	28
3	**3**	THF	60	12	36 (1.60)	20
4	—	THF	60	12	28 (1.24)	10
5	$NiCl_2(PPh_3)_2$	THF	60	12	22 (0.98)	6
6	$NiCl_2$	THF	60	12	33 (1.46)	20
7[b]	**1**	THF	60	12	40 (1.78)	20
8	**1**	THF	25	12	4 (0.18)	nd
9	**1**	THF	60	6	26 (1.16)	13
10[c]	**1**	THF	60	12	40 (1.78)	26
11	**1**	Dioxane	60	12	41 (1.83)	23
12	**1**	DME	60	12	22 (0.98)	10
13	**1**	THF	60	48	48 (2.14)	58
14	**1**	**THF**	**80**	**12**	**54 (2.40)**	**61**
15	**1**	THF	80	48	58 (2.58)	52
16[d]	**1**	THF	80	72	458 (2.04)	51

[a] Reaction conditions: AB (1 mmol), Ni complex (1 mol%), and solvent (1 mL); the yield of borazine was determined by ^{11}B NMR with $NaBPh_4$ (0.01 mmol) as an internal standard. [b] **1** (0.5 mol%). [c] Hg (100 equiv. w.r.t 1). [d] AB (10 mmol) and **1** (0.005 mol%).

trimethyl ammonia borane ($NMe_3{\cdot}BH_3$), no H_2 gas was generated under the mentioned reaction conditions (see SI, Fig. S42 and S43). Similarly, under the same conditions, complex **2** showed similar catalytic H_2 yield, whereas complex **3** exhibited lower catalytic activity, producing 36 mL of H_2 (1.6 equiv.) with 20% yield of BZ (entries 2 and 3). The significance of the molecular Ni complex was underscored by the low H_2 evolution and poor BZ selectivity obtained without a catalyst or with Ni precursors ($NiCl_2(PPh_3)_2$ and $NiCl_2$), leading us to pursue further study with complex **1** (entries 4–6). Notably, decreasing the loading of complex **1** to 0.5 mol% delivered 40 mL H_2 with only 20% BZ yield under the optimised conditions, indicating that although lower catalyst loading sustains gas evolution, it compromises with product selectivity (entry 7). Furthermore, decreasing the reaction temperature to 25 °C or shortening the reaction time to 6 h resulted in considerably lower H_2 production and poor BZ yield (entries 8 and 9). To further confirm the homogeneity of complex **1**, a mercury drop test was carried out under the standard conditions, resulting in no loss of catalytic activity (40 mL of H_2, 26% yield of BZ) (entry 10). However, when PPh_3 was introduced as an additive, the catalytic activity dropped sharply, comparable to that of the blank reaction in entry 4, Table 1 (see SI, Fig. S39). Screening various solvents, such as dioxane, DME, diethyl ether, or toluene, shows lower catalytic activity compared to THF under the optimised reaction conditions (entries 11 and 12, see SI, Table S1). When the reaction time was extended to 48 h, 48 mL of H_2 evolution was recorded along with 58% BZ yield (entry 13). To improve further selectivity, when performing the reaction at a higher temperature, 80 °C, 54 mL of H_2 (2.4 equiv.) with the highest yield of BZ (61%), along with PBZ formation, was achieved, as confirmed by ^{11}B NMR (27 ppm) and IR spectroscopy (see SI, section 5.5).[12] To witness the maximum H_2 evolution, under the Ni-based catalytic system, increasing both the reaction temperature and time to 80 °C and 48 h, respectively, leads to generating 58 mL of H_2 (2.58 equiv.), although lowering the BZ yield to 52% (entry 15). Importantly, to demonstrate the practical applicability, the catalyst loading of **1** was reduced to 0.005 mol%, under which 10 mmol of AB underwent efficient dehydrogenation to produce 458 mL of H_2 with a 51% yield of BZ, achieving the highest TON of 40 738 (entry 16, see SI, section 5.6).

Encouraged by the promising catalytic activity of complex **1**, we next evaluated its durability for H_2 production under the optimised conditions. Utilising only 1 mol% of complex **1** loading, the catalytic activity of producing H_2 remained active over eight consecutive cycles, generating a total of 414 mL H_2 with an overall TON of 1843 (Scheme 3a, see SI, section 5.1). Further monitoring the reaction progress through H_2 gas evolution revealed a fast initial rate, corresponding to an initial TOF of 298 h^{-1}, highlighting the high catalytic efficiency during the initial period of dehydrogenation (see SI, section 5.2). To understand the role of catalysts and aminoborane, a cyclohexene trapping experiment was carried out. During the catalytic dehydrogenation of AB to BZ, cyclohexene was employed as a trapping agent, and after chemical entrapment,

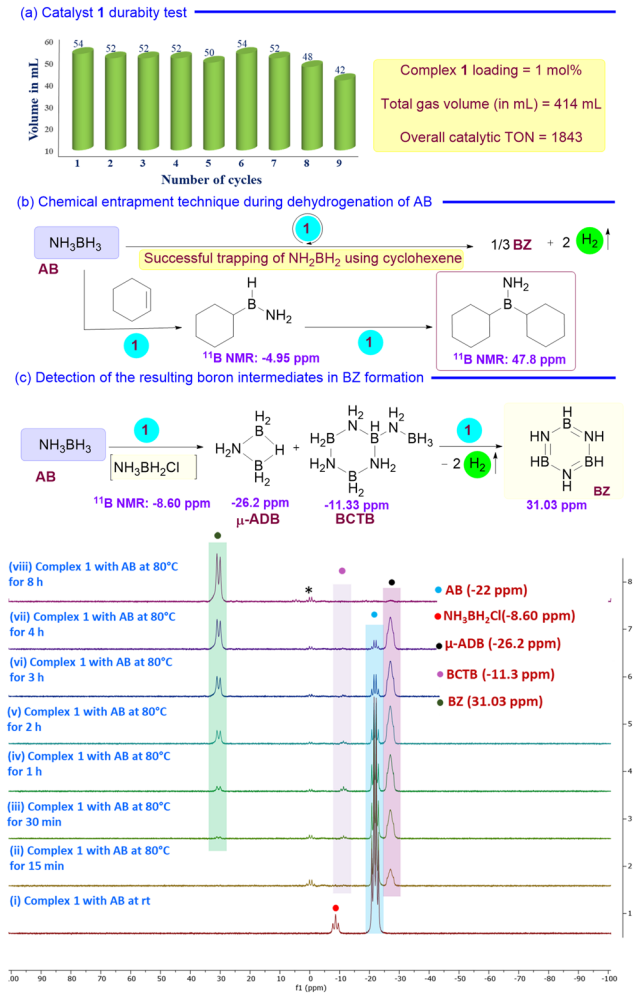

Scheme 3 (a) Catalyst **1** durability test; (b) chemical entrapment technique during dehydrogenation of AB; and (c) detection of the resulting boron intermediates in BZ formation. * Unidentified species.

it afforded $H_2NB(C_6H_{11})_2$, confirmed by a ^{11}B NMR peak at 47.8 ppm. This observation demonstrates that aminoborane (NH_2BH_2) is released as a reactive intermediate, which undergoes entrapment in solution rather than coordinating to the metal centre, thereby supporting an off-metal dehydrogenation pathway (Scheme 3b, see SI, section 5.3). In a metal-centred (on-metal) pathway, the aminoborane intermediate is expected to remain coordinated to the metal or proceed through subsequent metal-mediated transformation. As a result, its availability to react with an external alkene would be significantly reduced.[16]

Furthermore, the progress of the dehydrogenation reaction was monitored by ^{11}B NMR analysis by treating complex **1** (0.01 mmol) with AB (0.1 mmol) in THF/C_6D_6 (1 : 1). At room temperature, a transient intermediate NH_3BH_2Cl was initially detected at δ = −8.60 ppm, along with the unreacted AB.[28] However, upon heating to 80 °C for 15 min to 4 h, the signal for NH_3BH_2Cl disappeared, and new signals emerged at δ = 0.16 ppm (quartet) and δ = −11.33 ppm (triplet), attributable

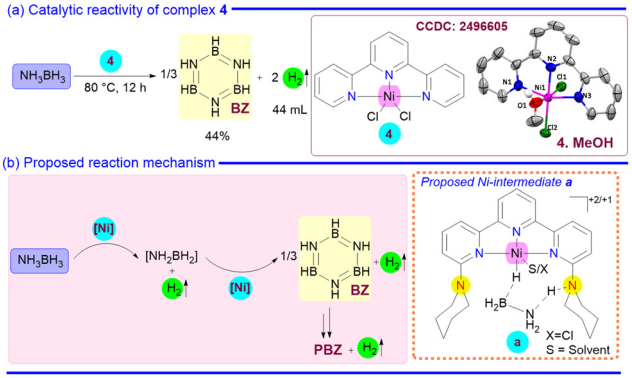

Scheme 4 (a) Catalytic reactivity of complex **4** and (b) proposed reaction mechanism.

to BCTB.[29] Simultaneously, a signal at δ = −26.2 ppm appeared, assigned to μ-ADB, along with a peak at δ = 31.03 ppm corresponding to the formation of BZ. Prolonging the reaction time up to 8 h at 80 °C resulted in the predominant formation of BZ with the consumption of AB, μ-ADB and BCTB (Scheme 3c, see SI, section 5.4).

To further examine the influence of the coordinated Lewis basic piperidine unit in the ligand framework of complex **1**, a piperidine-free terpyridine–Ni(II) dichloro analogue, complex **4**, was synthesised and confirmed by ESI-HRMS and single-crystal X-ray analyses. Upon utilizing complex **4** for the dehydrogenation of AB, 44 mL of H_2 (1.95 equiv.) and 44% yield of BZ were obtained at 80 °C over 12 h which indicates a significantly lower performance than that of complex **1** (Table 1, entry 14), indicating the pivotal role of the piperidine moiety in enhancing catalytic efficiency (Scheme 4a). Based on experimental observations and previous precedent literature, a mechanistic pathway has been proposed (Scheme 4b).[30–34] The reactivity of deuterated AB isotopologues (ND_3BH_3 and NH_3BD_3) was examined, which revealed a significantly slower formation of the corresponding deuterated BZ derivatives in comparison with AB (see SI, section 5.4). This highlights an efficient dehydrogenation of AB, which may occur through the outer-sphere cooperative activation of AB with the Ni centre and the piperidine N atom, as shown in **a**,[20,33,34] followed by a rapid hydride/proton recombination to liberate one equiv. of hydrogen gas with aminoborane. The transient aminoborane formed in this process is unstable and further undergoes self-condensation and isomerisation through intermediates such as BCTB and μ-ADB, ultimately affording BZ and PBZ as the thermodynamic end products with liberation of H_2 in the presence of an active catalyst.

3. Conclusions

In conclusion, this study demonstrates a Ni–NNN catalytic system **1** incorporating a piperidine-functionalized terpyridine backbone, which shows high efficiency for AB dehydrogenation, delivering up to 2.58 equiv. of H_2 with selectivity toward BZ. The catalysts operate under mild conditions with minimal catalyst loading and exhibit excellent reusability over eight consecutive cycles, maintaining their catalytic activity. Notably, a remarkable TON of 40 738 was achieved, representing the highest reported value among base-metal catalysts for this transformation. Further studies are in progress to obtain definitive experimental evidence supporting the cooperative role of the piperidine arm in complex **1** during the AB dehydrogenation process.

Conflicts of interest

There are no conflicts to declare.

Data availability

Supplementary information (SI): detailed experimental techniques and spectral and crystallographic information of complexes **2**, **3**, and **4**. See DOI: https://doi.org/10.1039/d5dt02924d.

CCDC 2496603–2496605 contain the supplementary crystallographic data of complexes 2, 3 and 4 respectively, for this paper.[35a–c]

Acknowledgements

P. D. thanks IISER Berhampur, Central Advanced Instrument Facility (CAIF) and Anusandhan National Research Foundation (ANRF), SERB, DST, India, for the financial support (CRG/2023/001880). B. M. thanks the University Grants Commission (UGC), India for the fellowship. A. M. thanks IISER Berhampur for the fellowship.

References

1 A. Staubitz, A. P. M. Robertson and I. Manners, *Chem. Rev.*, 2010, **110**, 4079–4124.
2 C. W. Hamilton, R. T. Baker, A. Staubitz and I. Manners, *Chem. Soc. Rev.*, 2009, **38**, 279–293.
3 U. B. Demirci, *Inorg. Chem. Front.*, 2021, **8**, 1900–1930.
4 D. Han, F. Anke, M. Trose and T. Beweries, *Coord. Chem. Rev.*, 2019, **380**, 260–286.
5 S. Chen, B. Magyari-Kope, C. Hsu, W. Woon and S. S. Liao, *Nat. Rev. Electr. Eng.*, 2025, **2**, 205–214.
6 M. Liu, L. Zhou, X. Luo, C. Wan and L. Xu, *Catalysts*, 2020, **10**, 1–34.
7 A. Rossin and M. Peruzzini, *Chem. Rev.*, 2016, **116**, 8848–8872.
8 X. Zhang, L. Kam, R. Trerise and T. J. Williams, *Acc. Chem. Res.*, 2017, **50**, 86–95.
9 I. Ortega-Lepe, A. Rossin, P. Sánchez, L. L. Santos, N. Rendón, E. Álvarez, J. López-Serrano and A. Suárez, *Inorg. Chem.*, 2021, **60**, 18490–18502.
10 D. Himmelbauer, F. Müller, C. Schweinzer, F. Casas, B. Pribanic, G. Le Corre, D. Thöny, M. Trincado and H. Grützmacher, *Chem. Commun.*, 2023, **60**, 885–888.

11 M. J. Cross, M. A. Sajjad, S. A. Macgregor and A. S. Weller, *Angew. Chem., Int. Ed.*, 2025, **64**, e202500019.
12 P. Jurt, J. J. Gamboa-Carballo, C. Schweinzer, D. Himmelbauer, D. Thöny, T. L. Gianetti, M. Trincado and H. Grützmacher, *Dalton Trans.*, 2024, **53**, 14212–14218.
13 M. Boudjelel, E. D. Sosa Carrizo, S. Mallet-Ladeira, S. Massou, K. Miqueu, G. Bouhadir and D. Bourissou, *ACS Catal.*, 2018, **8**, 4459–4464.
14 M. Hasenbeck, J. Becker and U. Gellrich, *Angew. Chem., Int. Ed.*, 2020, **59**, 1590–1594.
15 J. R. Vance, A. P. M. Robertson, K. Lee and I. Manners, *Chem. Eur. J.*, 2011, **17**, 4099–4103.
16 R. T. Baker, J. C. Gordon, C. W. Hamilton, N. J. Henson, P.-H. Lin, S. Maguire, M. Murugesu, B. L. Scott and N. C. Smythe, *J. Am. Chem. Soc.*, 2012, **134**, 5598–5609.
17 J. F. Sonnenberg and R. H. Morris, *ACS Catal.*, 2013, **3**, 1092–1102.
18 A. Glüer, M. Förster, V. R. Celinski, J. Schmedt auf der Günne, M. C. Holthausen and S. Schneider, *ACS Catal.*, 2015, **5**, 7214–7217.
19 C. Lichtenberg, M. Adelhardt, T. L. Gianetti, K. Meyer, B. de Bruin and H. Grützmacher, *ACS Catal.*, 2015, **5**, 6230–6240.
20 H. Takahashi, T. Watanabe and H. Tobita, *Chem. Lett.*, 2018, **47**, 296–299.
21 S. Todisco, L. Luconi, G. Giambastiani, A. Rossin, M. Peruzzini, I. E. Golub, O. A. Filippov, N. V. Belkova and E. S. Shubina, *Inorg. Chem.*, 2017, **56**, 4296–4307.
22 J. K. Pagano, J. P. W. Stelmach and R. Waterman, *Dalton Trans.*, 2015, **44**, 12074–12077.
23 P. Bhattacharya, J. A. Krause and H. Guan, *J. Am. Chem. Soc.*, 2014, **136**, 11153–11161.
24 R. J. Keaton, J. M. Blacquiere and R. T. Baker, *J. Am. Chem. Soc.*, 2007, **129**, 1844–1845.
25 A. Mohanty, S. R. Rout, R. Dandela and P. Daw, *Chem. Commun.*, 2024, **60**, 416–419.
26 A. Mohanty, G. Kenguva, R. Dandela and P. Daw, *ChemCatChem*, 2025, **17**, e01005.
27 S. T. Sahoo, A. Mohanty, R. Sharma and P. Daw, *Dalton Trans.*, 2023, **52**, 15343–15347.
28 H. K. Lingam, C. Wang, J. C. Gallucci, X. Chen and S. G. Shore, *Inorg. Chem.*, 2012, **51**, 13430–13436.
29 H. A. Kalviri, F. Gärtner, G. Ye, I. Korobkov and R. T. Baker, *Chem. Sci.*, 2015, **6**, 618–624.
30 E. Lu, Y. Yuan, Y. Chen and W. Xia, *ACS Catal.*, 2013, **3**, 521–524.
31 S. Bhunya, T. Malakar, G. Ganguly and A. Paul, *ACS Catal.*, 2016, **6**, 7907–7934.
32 V. Pons, R. T. Baker, N. K. Szymczak, D. J. Heldebrant, J. C. Linehan, M. H. Matus, D. J. Grant and D. A. Dixon, *Chem. Commun.*, 2008, **48**, 6597–6599.
33 A. Al-Kukhun, H. T. Hwang and A. Varma, *Int. J. Hydrogen Energy*, 2013, **38**, 169–179.
34 S. Bhunya, P. M. Zimmerman and A. Paul, *ACS Catal.*, 2015, **5**, 3478–3493.
35 (*a*) CCDC 2496603 (Complex 2): Experimental Crystal Structure Determination, 2025, DOI: 10.5517/ccdc.csd.cc2psxl0; (*b*) CCDC 2496604 (Complex 3): Experimental Crystal Structure Determination, 2025, DOI: 10.5517/ccdc.csd.cc2psxm1; (*c*) CCDC 2496605 (Complex 4): Experimental Crystal Structure Determination, 2025, DOI: 10.5517/ccdc.csd.cc2psxn2.